Available online at www.sciencedirect.com
ScienceDirect
Applied Catalysis B: Environmental 82 (2008) 255–263
APPLIED CATALYSIS B: ENVIRONMENTAL
www.elsevier.com/locate/apcatb

Direct NO decomposition over $La_{2-x}Ba_xNiO_4$ catalysts containing $BaCO_3$ phase

Yujun Zhu [a,b], Dong Wang [a], Fulong Yuan [a,*], Guo Zhang [a,b], Honggang Fu [a]

[a] *Heilongjiang Province Key Laboratory of Photoelectric, Energy and Environmental Materials, School of Chemistry and Materials, Heilongjiang University, 150080 Harbin, China*
[b] *State Key Laboratory of Theoretical and Computational Chemistry, Jilin University, 130021 Changchun, China*

Received 10 January 2007; received in revised form 12 January 2008; accepted 26 January 2008
Available online 7 February 2008

Abstract

$La_{2-x}Ba_xNiO_4$ ($x \leq 1.2$) catalysts have been prepared by citrate method. XRD patterns and IR spectra indicate that with the doping of Ba, more $BaCO_3$ appears and perovskite-like structure is seriously distorted. In directly decomposing 4% NO, the highest N_2 yield is achieved with $La_{1.2}Ba_{0.8}NiO_4$ composed of perovskite-like structure phase and $BaCO_3$ in the absence/presence of oxygen. The results of iodometry and H_2-TPR reveal that the increase in Ba causes the increase in Ni^{3+} content. O_2-TPD and NO adsorption tests confirm that Ba doping resulted in the increase in oxygen vacancy (Vo). Thus, the redox capability and the amount of Vo are enhanced. It is suggested that the $BaCO_3$ phase, NO_x storage component, contributes to the increase in activity by NO-TPD, NO_2-TPD and in situ DRIFT. Thus, $BaCO_3$ plays an important role in quickening up the run of catalytic NO decomposition recycle.
© 2008 Elsevier B.V. All rights reserved.

Keywords: Nitrogen oxide; Direct decomposition; $La_{2-x}Ba_xNiO_4$; Perovskite-like oxide

1. Introduction

Nitrogen oxides (NO_x) are serious pollutants in the earth's atmosphere in the sense that they are extremely toxic to the human body and also harmful to the environment. Therefore, the removal of NO_x is one of the key research projects in the protection of our environment. NO direct decomposition is the most desirable way of removing NO_x since it does not involve the addition of a reductant and the products of the reaction (N_2 and O_2) are nontoxic [1]. However, its decomposition is not only extremely slow, but it is also, especially in the presence of oxygen, more complicated by a series of fast competing reactions producing toxic nitrogen dioxide, or nitrous oxide [2].

Mixed oxides, which have the perovskite and related structures, have drawn much attention as useful catalysts for NO removal [2–13]. Perovskite-like oxides have the general formula A_2BO_4, and its structure can be described as containing alternate layering of perovskite (ABO_3) and rock-salt (AO) units [12]. These oxides (A_2BO_4) as well as perovskite (ABO_3) offer an opportunity to control the oxidation state of the B-site transition metal (the redox properties) and the oxygen stoichiometry by partial substitution of the A-and/or B site cations [12]. Although the catalytic activity of them is higher than that of single perovskite (ABO_3) in some reactions, compared to the literature about ABO_3-type mixed oxides, few papers concerning A_2BO_4-type mixed oxides catalysts in NO removal have been reported [11,14,15]. However, all these mixed oxide catalysts lack high activity for industrial application, partly because the formed oxygen adsorbed strongly on active site of catalyst resulting in difficult regeneration of active site. So, it is a key factor to improve the regeneration of active site.

For the mechanism of NO decomposition over non-noble metal, it is traditionally accepted that the formation of N_2 and O_2 occurred through reactions of $2NO_{(g)} \rightarrow N_2O_{(a)} \rightarrow N_{2(g)}$ and $O_{(a)} + O_{(a)} \rightarrow O_{2(g)}$, respectively [3,7,16–21]. Recently, it was found that $NO_{2(a)}/NO_{3(a)}$ species was strongly adsorbed on catalyst surface during NO decomposition [7,21–26], indicating that NO_2(a)/NO_3(a) species might be an intermediate in NO decomposition. Similarly, Zhu et al. [27] found that both NO_2 and O_2 were mainly formed on the catalyst surface by the way of

* Corresponding author. Tel.: +86 451 86608610; fax: +86 451 86673647.
E-mail addresses: yujunzhu@hlju.edu.cn (Y. Zhu), fulongyuan2000@yahoo.com (F. Yuan).

0926-3373/$ – see front matter © 2008 Elsevier B.V. All rights reserved.
doi:10.1016/j.apcatb.2008.01.025

$NO + O_{(a)} \leftrightarrow NO_{2(a)}$ and $2NO_{2(g)} \leftrightarrow 2NO_{(g)} + O_{2(g)}$ over perovskite-like oxides. Thus, it can be concluded that the formation of NO_2 plays an important role in NO decomposition. Therefore, the activity may be promoted by accelerative transformation and/or decomposition of the NO_2. Interestingly, a series of research results show that Pt-Ba/MO perform good capability in storing NO_x in NO_x storage-reduction (NSR) catalysts in which $BaCO_3$ and BaO are the storage components as $Ba(NO_3)_2$ or barium-nitro phase on surface [21,28–35], especially in storing NO_2 [28–31,35]. So the presence of $BaCO_3$ in perovskite-like oxides may affect the catalytic activity.

In the present study, direct decomposition of NO in high concentration over La_2NiO_4 perovskite-like oxide doped with Ba at La site ($La_{2-x}Ba_xNiO_4$) containing $BaCO_3$ phase was investigated in the absence/presence of oxygen. $La_{1.2}Ba_{0.8}NiO_4$ exhibits an excellent catalytic performance for NO decomposition, which was attributed to increasing and regenerating rapidly the oxygen vacancy (Vo) and storage capability of $BaCO_3$ for the NO_2 formed intermediate species.

2. Experimental

2.1. Preparation of catalyst

The samples, $La_{2-x}Ba_xNiO_4$ ($x \leq 1.2$), were prepared by citrate combustion method as described elsewhere [27]. Briefly, to an aqueous solution of La^{3+}, Ba^{2+}, and Ni^{2+} nitrates with appropriate stoichiometry, a solution of 50% citric acid in excess amount (molar ratio) was added. The resulting solution was evaporated to dryness, and then the precursors were calcined at 573 and 873 K for 1 h, respectively. Finally, the precursors were palletized and calcined at 1173 K in air for 6 h, and then the synthesized pellets were pulverized to 40–60 mesh size.

2.2. Characterization of catalyst

X-ray diffraction patterns (XRD) of the catalysts were obtained with a D/MAX-3B X-ray diffraction meter (Rigaku Co.) at room temperature, using Cu Kα radiation combined with Ni-filter.

The fourier transform infrared (FTIR) measurements of the catalysts were carried out in transmission mode pressed in the form of a KBr pellet, using a Equinox55 FTIR spectrometer (Bruker) operating at 2 cm^{-1} resolution.

The average oxidation number of Ni ions and the content of Ni^{3+} were determined by the chemical analysis using the method of iodometry [36,37] according to the procedures adopted by Yu et al. [38].

Temperature programmed reduction with hydrogen (H_2-TPR) was carried out in a conventional self-made apparatus equipped with TCD as a detector. The sample (0.0300 g) was reduced with a 5% (volume) H_2/N_2 mixture (25 cm^3/min) by heating from room temperature to 1173 K at a rate of 10 K/min.

Temperature programmed desorption of O_2 (O_2-TPD) experiments were performed in the self-made apparatus according to the following procedures: the sample (0.3000 g) was first heated up to 1073 K in O_2 with ramp rate 20 K/min and kept at 1073 K for 1 h, and then cooled to room temperature in O_2, finally heated to 1173 K at rate of 10 K/min in a flow of He (15 ml/min) recording the O_2-TPD spectra.

Temperature programmed desorption of NO (NO-TPD) and temperature programmed desorption of NO_2 (NO_2-TPD) were performed on a Netzsch QMS403C thermoanalyzer with mass spectrometry (MS). About 0.0200 g of the sample was first treated in Ar at 1073 K for 1 h and cooled to 353 K in same atmosphere, and then swept with 4% (volume) NO or 4% NO_2 diluted with helium for the adsorption of NO or NO_2 for 2 h at atmospheric pressure and the adsorption spectra were recorded with MS. Then, the sample was swept with Ar at a rate of 30 cm^3/min for 2 h in order to remove the residual NO or NO_2. Finally, the sample was heated to 1173 K at a rate of 10 K/min in Ar to record the TPD spectra with MS. In NO-TPD of $La_{1.2}Ba_{0.8}NiO_4$, 0.100 g sample was used.

The specific surface area of the samples was measured by N_2 adsorption at 77 K with a Micromeritics ASAP 2010 instrument.

In situ diffuse reflectance infrared fourier transform (DRIFT) experiments were conducted using a Digilab FTS–3000 FTIR spectrometer equipped with a continuous flow reaction chamber (Harrick Scientific Praying Mantis DRIFT optics and cell). The experiment was performed by introducing 2000 ppm NO + 5% O_2 in He, with a total gas flow of 50 ml/min over the powder sample. The background spectrum was measured at the temperature where $NO + O_2$ mixture gas adsorption was studied [39,40].

2.3. Catalytic procedure

Direct decomposition of NO was performed with a conventional fixed-bed reactor with a 6 mm-diameter quartz glass tube. Gaseous mixtures of 4% NO or 1% NO diluted with He were fed to the catalyst bed. In each experiment, 0.5 g of the catalyst (40–60 mesh) without dilution was set in the reactor by using quartz wool. The feed rate of the reactant was at W/F = 0.3–1.2 $g_{cat.}$ s cm^{-3}, where W and F stand for the catalyst weight and the flow rate of gaseous mixtures of NO, respectively. In the coexistence of O_2 experiment, 0.5 g of the catalyst was adopted and the gas reactant of the 4% NO and 2% O_2 were fed at 25 and 15 cm^3/min, respectively. The gas composition was analyzed before and after the reaction by an online gas chromatography, using molecular sieve 5A column for separating NO, N_2 and O_2. In any particular run, the data were recorded after at least 1 h on stream being allowed after each temperature change to ensure that the equilibrium of catalytic reaction was reached. The activity of NO decomposition was evaluated by the following equations:

$$\text{NO conversion}\% = \frac{[\text{NO}]_{\text{in}} - [\text{NO}]_{\text{out}}}{[\text{NO}]_{\text{in}}} \times 100\%$$

$$\text{N}_2\text{yield}\% = \frac{2[\text{N}_2]_{\text{out}}}{[\text{NO}]_{\text{in}}} \times 100\%$$

$$\text{O}_2\text{yield}\% = \frac{2[\text{O}_2]_{\text{out}}}{[\text{NO}]_{\text{in}}} \times 100\%$$

where $[NO]_{in}$ was the concentration of NO measured before the reaction, $[NO]_{out}$, $[N_2]_{out}$ and $[O_2]_{out}$ were the concentration of NO, N_2 and O_2 measured after the reaction, respectively.

3. Results and discussion

3.1. Study of powder X-ray diffraction and IR spectra

The X-ray diffraction patterns of the substituted perovskites-like catalysts ($La_{2-x}Ba_xNiO_4$ ($x \leq 1.2$)) almost show the same lines that La_2NiO_4 ($2\theta = 31.32$, 32.74, 42.52, 43.66 and 47.00°, PDF 34-0314) suggested the K_2NiF_4-type structure (Fig. 1). However, it is observed that a XRD line shifts to smaller 2θ angle values when the Ba amount ($0 \leq \times \leq 0.4$) increases. This indicates that Ba^{2+} is incorporated into the lanthanum site, which contributes to the larger radius of Ba^{2+} [41]. Furthermore, a decrease intensity and a broad shape in the characteristic diffraction line of La_2NiO_4 phase with further increasing Ba amount ($x \geq 0.6$) is also observed, which reveals that the crystal structure is seriously distorted with the increase in Ba content. Meanwhile, $BaCO_3$ (witherite phase), a new phase, appears at $2\theta = 23.7$, 24.3, 34.1 and 44.86° (PDF 05-0378) when x equals 0.6, which almost becomes the main phase when x exceeds 1.0 (Fig. 1). The XRD patterns of $La_{2-x}Ba_xNiO_4$ catalysts were magnified between $2\theta = 23$ ° and $2\theta = 25$ ° and was attached on the left side in Fig. 1, in which the characteristic diffraction lines of $BaCO_3$ are obviously found when $x \geq 0.6$. Therefore, when x value exceeds 0.6, $La_{2-x}Ba_xNiO_4$ represents molar ratio among different metals rather than molecular formula. The results from XRD are summarized in Table 1.

In order to obtain further insight into this aspect, IR spectra of $La_{2-x}Ba_xNiO_4$ ($x \leq 1.2$) catalysts were recorded and displayed in Fig. 2. According to the literature, the main absorptions in the regions 510–460 cm^{-1} assigned to A–O_{II}–B characteristic vibrational frequency of A_2BO_4 prove that these samples have K_2NiF_4-type structure [14,42]. When x value increases in range of 0.0–0.4, the band shifts from 507.2 to 495.6 cm^{-1} due to the larger radius of Ba^{2+} than that of La^{3+}, which indicates that Ba^{2+} is incorporated into the lanthanum site. The band at 510–460 cm^{-1} becomes broader with weaker intensities at $0.8 \leq x \leq 1.2$, which proves that the K_2NiF_4-type structure is seriously distorted. The $La_{2-x}Ba_xNiO_4$ ($x \geq 0.6$) catalysts reveal the four characteristic vibrational frequencies of $BaCO_3$, a strong band at 1427 cm^{-1}, a small one at 1056 cm^{-1}, and two sharp bands at 854 and 690 cm^{-1} [43,44] (Fig. 1). And the relative intensities of these bands increase with x value in agreement with XRD results. There is almost no appearance of the bands associated with $BaCO_3$ in the IR spectrum of the $La_{1.6}Ba_{0.4}NiO_4$, which is also agreed with the results of XRD shown in Fig. 1.

Table 1
Crystal structure, surface area and average oxidation number of nickel of $La_{2-x}Ba_xNiO_{4+\delta}$

Catalyst	Structure	SSA/m^2 g^{-1}	Oxidation number of nickel	δ[a]
La_2NiO_4	K_2NiF_4	4.9	+2.15	+ 0.076
$La_{1.8}Ba_{0.2}NiO_4$	K_2NiF_4	3.6	+2.08	−0.058
$La_{1.6}Ba_{0.4}NiO_4$	K_2NiF_4	5.0	+2.13	−0.14
$La_{1.4}Ba_{0.6}NiO_4$	K_2NiF_4 + $BaCO_3$	5.5	+2.25	–
$La_{1.2}Ba_{0.8}NiO_4$	K_2NiF_4 + $BaCO_3$	6.6	+2.37	–
$LaBaNiO_4$	K_2NiF_4 + $BaCO_3$	7.3	+2.20	–
$La_{0.8}Ba_{1.2}NiO_4$	K_2NiF_4 + $BaCO_3$	6.0	+2.07	–

[a] δ: oxygen nonstoichiometry in $La_{2-x}Ba_xNiO_{4+\delta}$.

3.2. Effects of Ba contents on NO decomposition activity

The yield of N_2 in direct decomposition of 4% NO over $La_{2-x}Ba_xNiO_4$ at different temperatures is showed in Fig. 3. It increases with temperature in the range of $0.0 \leq x \leq 1.2$. For the series of $La_{2-x}Ba_xNiO_4$ catalysts, the catalytic activity in the range of $0.0 \leq x \leq 0.8$ increases with x at each temperature point. In the range of $0.8 \leq x \leq 1.2$, however, the catalytic activity of NO decomposition decreases, and the catalytic activity decreases rapidly at $1.0 \leq x \leq 1.2$. In the present study, these catalysts have lower surface area in range of 3.6–7.3 m^2/g as summarized in Table 1. Thus, the difference of catalytic performance among all catalysts is not mainly due to the surface area. The $La_{2-x}Ba_xNiO_4$ catalyst with x equaling 0.8 performs the highest activity. The N_2 yield attained a value of 88.9%, 78.8% and 62.5% during the initial 30 min and it is

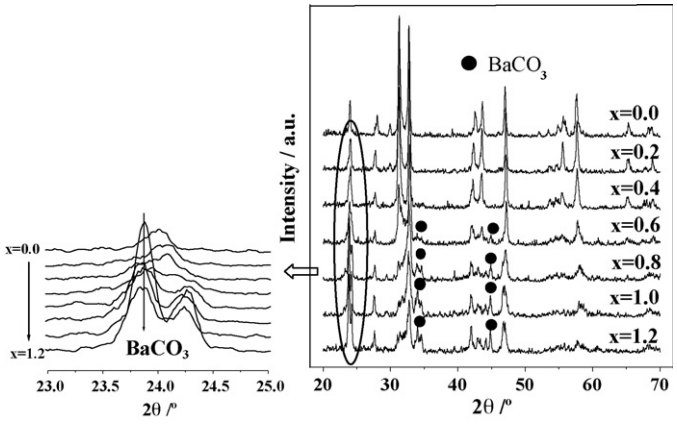

Fig. 1. XRD patterns of $La_{2-x}Ba_xNiO_4$ ($x \leq 1.2$).

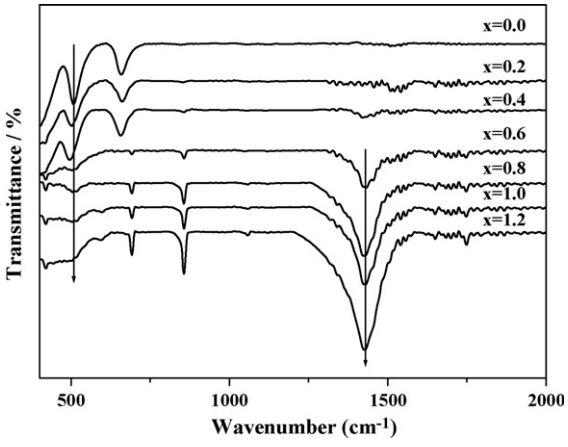

Fig. 2. FT-IR spectra of $La_{2-x}Ba_xNiO_4$ ($x \leq 1.2$).

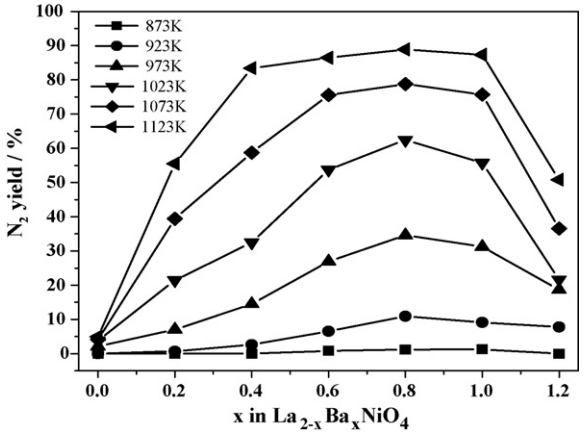

Fig. 3. N_2 yield as a function of x over $La_{2-x}Ba_xNiO_4$ (4% NO, catalyst: 0.5 g, W/F = 1.2 $g_{cat.}$ s cm^{-3}).

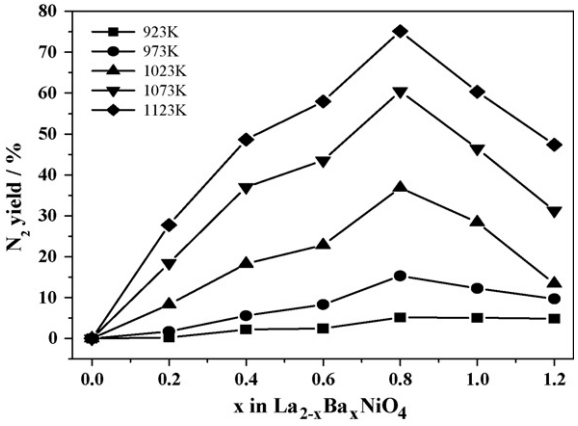

Fig. 5. Yield of N_2 as a function of x over 0.5 g $La_{2-x}Ba_xNiO_4$ in presence of O_2 (NO: 4%, 25 cm^3/min; O_2: 2%, 15 cm^3/min; W/F = 0.75 $g_{cat.}$ s cm^{-3}).

quite stable over 15 h at 1123, 1073 and 1023 K respectively. The N_2 and O_2 yields with reaction time over $La_{1.2}Ba_{0.8}NiO_4$ catalyst at 1073 K are shown in Fig. 4. As far as we know, this is almost higher than that of any mixed oxides reported, although the NO concentration is three times higher than that of others. Generally, NO concentration ($\leq 1\%$) was involved in the catalytic activity in literatures [7,27]. In this study, the activity of 1% NO direct decomposition over $La_{1.2}Ba_{0.8}NiO_4$ has also been investigated and NO can be almost completely decomposed to N_2 at 1123 K.

In addition, the activity of $La_{2-x}Ba_xNiO_4$ ($x \leq 1.2$) in presence of oxygen has also been investigated, as shown in Fig. 5. The relation between N_2 yield and x value in presence of oxygen is identified with that in absence of O_2. $La_{1.2}Ba_{0.8}NiO_4$ also performs the highest activity in NO decomposition among $La_{2-x}Ba_xNiO_4$ ($x \leq 1.2$) catalysts, and 60% NO (4%) could be converted to N_2 at 1073 K and 75% NO (4%) to N_2 at 1123 K even if 2% O_2 (volume) was added in the feed. It notes that the activity increases more sharply when x varies from 0.4 to 0.6 with the appearance of $BaCO_3$ phase. In particular, the presence of $BaCO_3$ does not depress the activity until x = 1.0, be there oxygen in the feed or not. Notably, when $BaCO_3$ phase appears in $La_{1.2}Ba_{0.8}NiO_4$, it exhibits the highest activity in NO decomposition reaction in presence/absence of oxygen in the feed. Thus, $BaCO_3$ phase may play some role in NO decomposition reaction.

Some experiments have been designed, in order to investigate whether $BaCO_3$ can serve as the function of improving the activity of perovskite-like oxides. The catalyst has been prepared by simply mixing 0.5 g $La_{1.6}Ba_{0.4}NiO_4$ (without $BaCO_3$ phase) and 0.1 g $BaCO_3$, and its activity has been evaluated in NO decomposition under the same conditions as that of $La_{2-x}Ba_xNiO_4$. The results are shown in Fig. 6. Thus, it is seen that the mixture catalyst of $La_{1.6}Ba_{0.4}NiO_4$ and $BaCO_3$ performs higher activity than either $La_{1.6}Ba_{0.4}NiO_4$ or $BaCO_3$, which is obvious at lower reaction temperature (Fig. 6). The yield of N_2 from the mixture catalyst of $La_{1.6}Ba_{0.4}NiO_4$ and $BaCO_3$ is about 15% higher than that of $La_{1.6}Ba_{0.4}NiO_4$ catalyst under 1023 K. This experiment confirms that $BaCO_3$ has the ability to enhance the catalytic activity of perovskite-like oxides in NO decomposition. Although 4.7% NO is decomposed to N_2 at 1073 K and 25% NO to N_2 at 1123 K over 0.5 g $BaCO_3$, there is not so much $BaCO_3$ in 0.5 g $La_{2-x}Ba_xNiO_4$ ($x \geq 0.6$). Therefore, the better activity performed by $La_{1.2}Ba_{0.8}NiO_4$ may result from the corporate effect of $BaCO_3$ and perovskite-like phase.

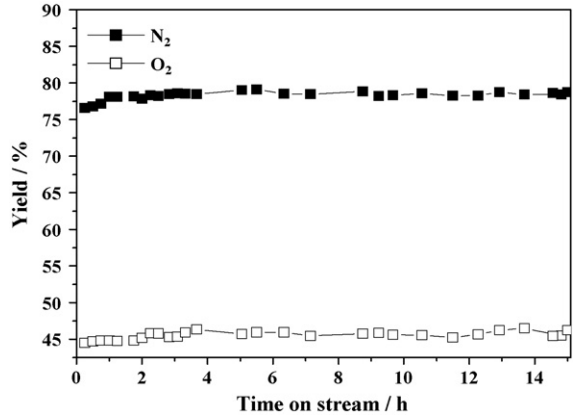

Fig. 4. Yield of N_2 and O_2 at 1073 K as a function of time on stream over $La_{1.2}Ba_{0.8}NiO_4$ (4% NO, catalyst: 0.5 g W/F = 1.2 $g_{cat.}$ s cm^{-3}).

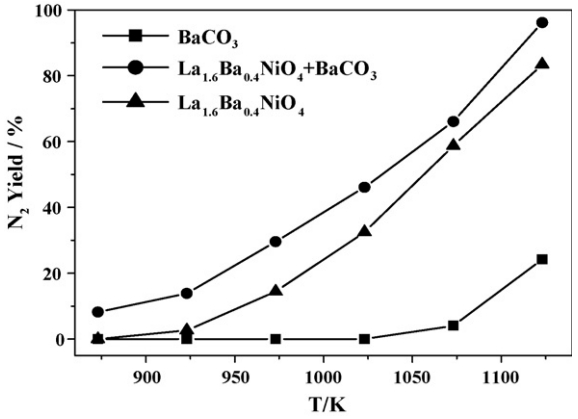

Fig. 6. Yield of N_2 with temperature over 0.5 g $BaCO_3$, 0.5 g $La_{1.6}Ba_{0.4}NiO_4$ and $La_{1.6}Ba_{0.4}NiO_4$ (0.5 g)/$BaCO_3$ (0.1 g) (4% NO, W/F = 1.2 $g_{cat.}$ s cm^{-3}).

When Ba content exceeds 1.0, the perovskite-like structure is distorted so severely that the active sites are reduced. As a result, the conversion of NO to N_2 falls off. As a whole, the Ba-substituted samples, in which $BaCO_3$ phase appears, show excellent performance in the decomposition of NO in high concentration.

3.3. Effects of Ba contents on defect structure of $La_{2-x}Ba_xNiO_4$

The Ni average oxidation number was determined by means of the back titration of iodine according to the literature [36-38]. The oxygen nonstoichiometry (δ) has been calculated on the assumption of presence of nickel as a mixture of Ni^{2+} and Ni^{3+} in $La_{2-x}Ba_xNiO_4$ ($x \leq 1.2$) shown in the last column of Table 1. Here, $La_{2-x}Ba_xNiO_{4+\delta}$ is represented as $La_{2-x}Ba_xNiO_4$. In respect that the average oxidation number of nickel is 2.15 ($\delta = +0.076$) for La_2NiO_4, it suggests that La_2NiO_4 without substituting Ba for La is rich in oxygen, and there will only be very few oxygen vacancies in the structure. Following the doping of Ba, the average oxidation number of nickel increases from 2.08 to 2.37 when x varies from 0.2 to 0.8 as shown in Table 1. It is well known that substitution of a bivalent metal cation for La^{3+} would bring about the decrease in positive charge. And the reduced positive charge could be balanced either by the formation of higher oxidation state ion at B site, i.e. $Ni^{2+} \rightarrow Ni^{3+}$, or by the formation of Vo [14,41]. In fact, the two cases often coexist. So the rise in Ni^{3+} content indicates that Ba^{2+} comes into A site. In this experiment, due to the formation of $BaCO_3$ phase, we cannot measure the oxygen nonstoichiomestry δ at $x \geq 0.6$ by iodometry to confirm the increase in Vo. However, it is seen in Table 1 that both Ni^{3+} content and oxygen nonstoichiomestry δ indeed increase when x varies from 0.2 to 0.4. Therefore, it is reasonable to speculate that the doping of Ba causes the increase in Ni^{3+} content and in the number of Vo at $x \leq 0.8$, which is beneficial to composition of active site of NO decomposition. And the speculation is confirmed by the following results of H_2-TPR, O_2-TPD and NO adsorption. However, when $x > 0.8$, Ni^{3+} content decreases with the further doping of Ba because a large part of Ba exists as $BaCO_3$. Although the overdoping of Ba does not destroy the matrix structure completely, the ratio of perovskite-like phase falls abruptly at $x \geq 1.0$.

As discussed above, more Ni^{3+} and Vo could be generated by substituting Ba for La properly, which is propitious for the increase in catalytic activity.

3.4. Effects of Ba contents on redox-capability and O_2-TPD of $La_{2-x}Ba_xNiO_4$

Results of hydrogen temperature programmed reduction experiments have been carried out on $La_{2-x}Ba_xNiO_4$ ($x \leq 1.2$) samples as reported in Fig. 7. All of H_2-TPR profiles of the catalysts show two reduction peaks. For La_2NiO_4, to which no Ba is added, no Vo is formed and there is excess oxygen (see Table 1), the first reduction peak ($T = 652$ K), then, is mainly ascribed to the reduction of excess oxygen. The second peak

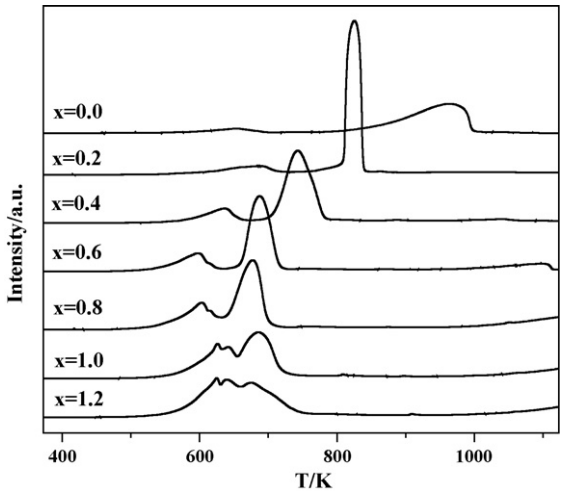

Fig. 7. H_2-TPR profiles of $La_{2-x}Ba_xNiO_4$ ($x \leq 1.2$).

($T = 965$ K) is ascribed to $Ni^{2+} \rightarrow Ni^0$ at high temperature region, which indicates the poor reducibility of lattice oxygen, i.e. the poor mobility of lattice oxygen [45]. For $La_{2-x}Ba_xNiO_4$ ($0 < x \leq 0.8$), oxygen vacancies are formed and some of Ni^{2+} ions are oxidized to Ni^{3+} with addition of Ba contents. Thus, the first reduction peak at a lower temperature is due to the reduction of $Ni^{3+} \rightarrow Ni^{2+}$ accompanying the reduction of chemical adsorptive oxygen [11,14]. To determine the final state of the sample after each reduction peak, when each reduction peak finished, the sample was analyzed by XRD [41]. Here, $La_{1.6}Ba_{0.4}O_4$ was selected as a sample because of no presence of $BaCO_3$. The XRD pattern of $La_{1.6}Ba_{0.4}O_4$ after the TPR experiment at 673 K is shown in Fig. 8. It is observed that the perovskite-like phase is preserved. Furthermore, a slight peak was found to shift towards lower 2θ angles (Fig. 8). This indicates that the reduction causes an expansion of the unit cell volume, which is predictable from the difference between the ionic radii of Ni^{3+} and Ni^{2+}. These results conduce us to assign the first peak to the reduction of Ni^{3+} to Ni^{2+} [41,46]. Table 2 lists the maximum temperature (T_1, T_2) and the area of each reduction peak and the corresponding reduction species. For $La_{2-x}Ba_xNiO_4$ ($0 < x \leq 0.8$), the temperature of the first reduction peak (T_1) decreases from 689 to 602 K and the reduction peak area increases with increasing Ba content from

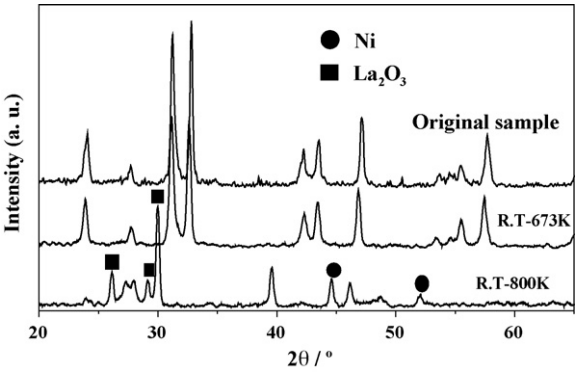

Fig. 8. XRD patterns for $La_{1.6}Ba_{0.4}NiO_4$ before and after reduction at different temperature.

Table 2
Data of H_2-TPR measurement of $La_{2-x}Ba_xNiO_4$

Catalyst	Data obtained from H_2-TPR			
	$Ni^{3+} \rightarrow Ni^{2+}$ T_1 (K)	$Ni^{3+} \rightarrow Ni^{2+}$ peak area	$Ni^{2+} \rightarrow Ni^0$ T_2 (K)	$Ni^{2+} \rightarrow Ni^0$ peak area
La_2NiO_4	652	90.3 [a]	965	886.5
$La_{1.8}Ba_{0.2}NiO_4$	689	177.1	826	1086.8
$La_{1.6}Ba_{0.4}NiO_4$	636	189.0	744	998.7
$La_{1.4}Ba_{0.6}NiO_4$	600	222.8	688	808.5
$La_{1.2}Ba_{0.8}NiO_4$	602	395.3	678	771.9

[a] The peak area is ascribed to the reduction of excess oxygen.

0.2 to 0.8. And the increase in the area of the first reduction peak with x ($0.2 \leq x \leq 0.8$) value also accounts for the increase in Ni^{3+} content as described above (Table 1). For $La_{2-x}Ba_xNiO_4$ ($0 \leq x \leq 0.8$), the second peak is ascribed to $Ni^{2+} \rightarrow Ni^0$, accompanying the reduction of lattice oxygen confirmed by the XRD patterns as above method [11,14,45]. In the XRD patterns of reduced $La_{1.6}Ba_{0.4}O_4$ sample, it is identified that Ni and La_2O_3 are mainly crystalline phases after 800 K. These results prove that the assign of the second reduction peak. While addition of Ba ($0 \leq x \leq 0.8$), the temperature of the second reduction peak (T_2) also decreases from 965 to 678 K with x value increase. Thus, the downward shift of the second peak reveals the improvement of the reducibility of lattice oxygen. It is concluded that the number of Ni^{3+} portion in the samples increases with Ba amount ($0.2 \leq x \leq 0.8$). It is obvious that the profiles of $LaBaNiO_4$ and $La_{0.8}Ba_{1.2}NiO_4$ are different from others. This is attributed to their different composition, so the profiles of them are not taken into consideration.

The O_2-TPD curves were obtained over $La_{2-x}Ba_xNiO_4$ ($x \leq 1.2$), and there were three O_2-desorption peaks (α, β and γ) respectively, as showed in Fig. 9. The peak appeared in range of 400–670 K could be attributed to the ordinarily chemically adsorbed oxygen (denoted as: α oxygen (O^{2-})). The peak at 670 –~1000 K corresponds to the desorption of the oxygen chemically adsorbed on oxygen vacancies (denoted as: β oxygen), namely, the oxygen is released by reduction of Ni^{3+} according to the following reaction: $2Ni^{3+} + O^{2-} \rightarrow 2Ni^{2+} + Vo + 1/2O_2$. The peak appeared at > ~1000 K might be attributed to the lattice oxygen

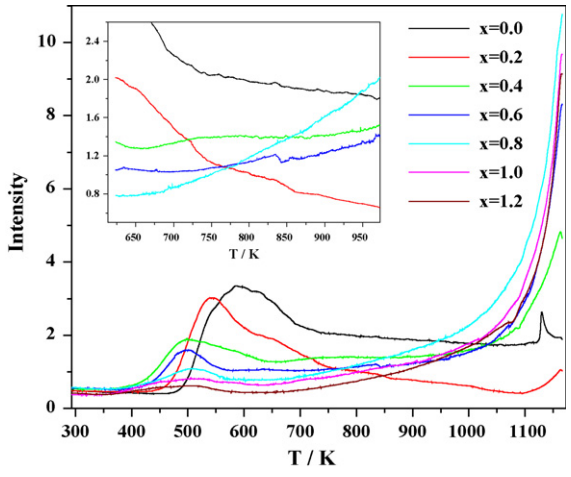

Fig. 9. O_2-TPD profiles of $La_{2-x}Ba_xNiO_4$ ($x \leq 1.2$).

associated with the redox of B ions (denoted as: γ oxygen) [3,11,15,47]. In Fig. 9, with the increase of x ($x = 0.0$–0.8), α peak area decreases, whereas β and γ peaks areas increase gradually, implying that oxygen vacancies and mobile lattice oxygen also increases. The β and γ oxygen desorption peaks are interesting for NO direct composition among the three oxygen desorption peaks [15]. No β oxygen desorption was detected and the area of γ oxygen desorption peak was very small over La_2NiO_4. The desorption area of β oxygen increased with the increase of Ba content at $0.2 \leq x \leq 0.8$, suggesting the increase of the number of oxygen vacancies. The amount of γ oxygen desorption also increases with x ($0.2 \leq x \leq 0.8$), and that the beginning temperature of the γ oxygen desorption peak shifted to lower temperature with the addition of Ba ($0.2 \leq x \leq 0.8$), implying the increase of the mobility of lattice oxygen. It should be noted that the peaks area of β and γ oxygen desorption over $La_{1.2}Ba_{0.8}NiO_4$ are the largest among all the samples. The O_2-TPD profiles of $LaBaNiO_4$ and $La_{0.8}Ba_{1.2}NiO_4$ are not discussed which is attributed to their different composition from others.

It seems that the Ba substitution promotes the redox capability of catalysts, increases of the number of oxygen vacancies and improves the mobility of lattice oxygen, which possibly leads to good catalytic performance. It partly accounts for the fact that $La_{1.2}Ba_{0.8}NiO_4$ performs excellent catalytic performance.

3.5. NO adsorption and NO-TPD

In order to investigate the performance of catalysts, the NO adsorption over $La_{2-x}Ba_xNiO_4$ has been measured as shown in Fig. 10. It is obviously seen that the addition of Ba improves the NO adsorption on $La_{2-x}Ba_xNiO_4$. When x varies from 0.0 to 0.8, the time to reach saturated adsorption increases from 30 to 50 min, and the ratio of NO adsorption grows from 9.09% ($x = 0.0$) to 19.33% ($x = 0.8$) (NO adsorption amount (mass): La_2NiO_4 9.09%, $La_{1.8}Ba_{0.2}NiO_4$ 10.74%, $La_{1.6}Ba_{0.4}NiO_4$ 13.09%, $La_{1.4}Ba_{0.6}NiO_4$ 15.64%, $La_{1.2}Ba_{0.8}NiO_4$ 19.33%, $LaBaNiO_4$ 12.49%). However, when Ba content increases to 1.0, the samples spend shorter time in attaining saturated adsorption, and the ratio of NO adsorption decreases to 12.49%. This is attributed to the poor performance of $BaCO_3$ in NO storage. Similar to the results reported by Prinetto et al. [30], bulk $BaCO_3$ performs poor capability in adsorbing NO during the experiment as shown in Fig. 10 (NO adsorption amount (mass) 6.02%). The results could involve surface Vo of $La_{2-x}Ba_xNiO_4$, which is the main active sites for NO adsorption

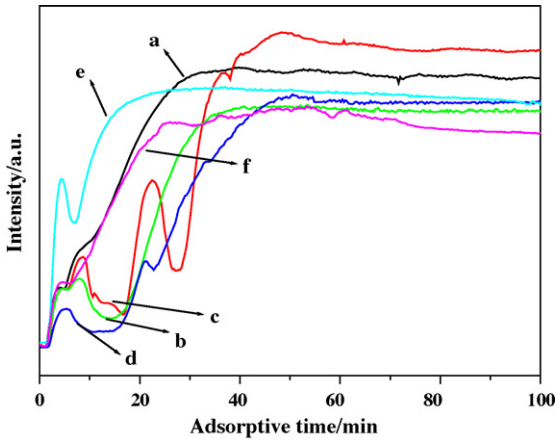

Fig. 10. NO adsorption profiles of $La_{2-x}Ba_xNiO_4$ at 353 K ((a) $x = 0.0$; (b) $x = 0.4$; (c) $x = 0.6$; (d) $x = 0.8$; (e) $x = 1.0$; (f) $BaCO_3$).

on the surface of perovskite-like oxides [3,4]. Here, the increase in the amount of NO adsorption also explains the continuous increase in the number of Vo when $x \leq 0.8$, which is in agreement with the results of O_2-TPD. Interestingly, the rule observed by NO adsorption agrees well with the sequence of activity of $La_{2-x}Ba_xNiO_4$ ($x = 0.0$–1.2) as shown in Fig. 3. In other words, $La_{1.2}Ba_{0.8}NiO_4$ has the highest activity in NO adsorption, so do it in NO decomposition. Therefore, the increase in the amount of Vo also contributes to the increase of NO adsorption, which can bring about the improvement in activity.

In addition, NO-TPD curves of $La_{1.2}Ba_{0.8}NiO_4$ have been measured as shown in Fig. 11. In the low temperature range, only small amount of NO desorption in company with N_2 and O_2 desorption is observed between 373 and 650 K, and the desorption amount of N_2 is more than that of O_2. This illustrates that NO has been dissociated before NO desorption. On the other hand, it is interesting that the large amount of NO and O_2 desorption are observed at 784 K. Furthermore, no desorption of N_2 is observed at this temperature. In general, NO desorption should be occurred at lower than higher temperature [13,14]. This means that some part of adsorbed NO may react with the oxygen dissociated by NO to form NO_x species that is adsorbed on the surface of the catalyst. Then, the NO_x species is decomposed to NO and O_2 at higher temperature. In experiment, it is observed that the yield of N_2 is smaller than the conversion of NO; however, it is larger than the yield of O_2 all the time for $La_{1.2}Ba_{0.8}NiO_4$ catalyst. Similarly, others have also noticed the same phenomenon [7,27], which has been confirmed that NO_2 and NO_2-derived species are important intermediates during NO decomposition process [7,23,25]. Hence, it is assumed that besides the oxygen adsorbed on Vo, the oxygen dissociated by NO also partly reacts with NO to form intermediates NO_2 species. Noticeably, NO_2 desorption does not occurred during NO-TPD of $La_{1.2}Ba_{0.8}NiO_4$ shown in Fig. 11. Thus, it indicates that NO_2 species may be stored on the surface of catalyst or dissociated rather than be desorbed into gas. Thus, Based on the composition of $La_{1.2}Ba_{0.8}NiO_4$ catalyst, $BaCO_3$ phase may play a key role in NO_2 species storage in the above process.

3.6. NO_2-TPD over $BaCO_3$ and $La_{1.2}Ba_{0.8}NiO_4$

Nowadays, many papers have reported that Pt-Ba/MO (MO = CeO_2, SiO_2, ZrO_2, MgO and Al_2O_3), in which $BaCO_3$ is the storage component [21,28–35], could store NO_x. And CO_2 desorption occurs at low temperature resulted from the different basicity of supports while $BaCO_3$ stores NO_2 as nitrates or nitrites. In order to investigate NO_2 species storage and dissociation over $BaCO_3$ without supports, the NO_2 adsorption and temperature programmed desorption over bulk $BaCO_3$ have been carried out as Piacentini's description [28]. In the NO_2 adsorption process, NO_2 can also be adsorbed on the bulk $BaCO_3$ without supports and reached saturated adsorption in 25 min (figure not shown). Moreover, the mass of $BaCO_3$ increases by 16.18% after NO_2 adsorption. In the process, however, no CO_2 escapes from $BaCO_3$. NO_2-TPD over $BaCO_3$ has also been investigated continuously as shown in Fig. 12(a). It can be seen that there is no NO_2 desorption within the temperature range. Instead, there is O_2 and NO evolution at 843 K, which indicates that NO_2 species adsorbed on $BaCO_3$ could be decomposed to NO and O_2 rather than be desorbed. At

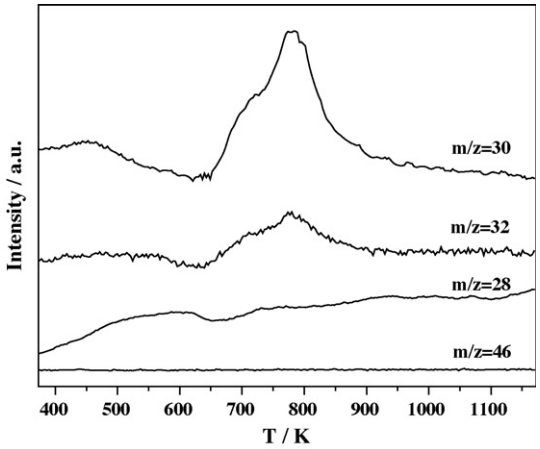

Fig. 11. NO-TPD profiles of $La_{1.2}Ba_{0.8}NiO_4$.

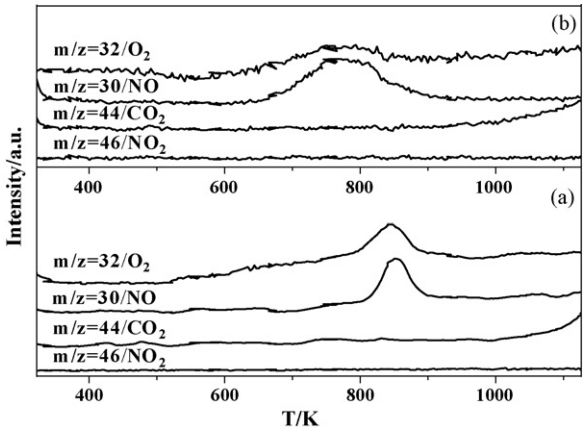

Fig. 12. NO_2-TPD profiles of $BaCO_3$ and $La_{1.2}Ba_{0.8}NiO_4$ ((a) $BaCO_3$; (b) $La_{1.2}Ba_{0.8}NiO_4$).

the same time, $BaCO_3$ adsorbing NO_2 showing the same thermal stability as $BaCO_3$ without adsorbing NO_2, does not release CO_2 until 973 K. In this process (temperature ranging from 323 to 1173 K), the mass of $BaCO_3$ decreases by only 0.73% due to its trace thermal decomposition beyond 973 K. Therefore, $BaCO_3$ still displays higher thermal stability after NO_2 adsorption and desorption. Briefly, bulk $BaCO_3$ could store NO_2 without releasing CO_2, and NO_2 species adsorbed on $BaCO_3$ could be easily decomposed to NO and O_2 rather than be desorbed. NO_2-TPD on $La_{1.2}Ba_{0.8}NiO_4$ is similar to that on $BaCO_3$ shown in Fig. 12(b). There is no NO_2 desorption, but NO and O_2 are released at 770 K. The temperature of NO and O_2 desorption over $La_{1.2}Ba_{0.8}NiO_4$ is lower than that of $BaCO_3$ illustrated in Fig. 12(a). And the temperature of CO_2 desorption also decreases to 900 K. This may result from the fact that the appearance of Ba-substituted La_2NiO_4 in $La_{1.2}Ba_{0.8}NiO_4$ influences the property of NO_2 desorbed on $BaCO_3$. It is pointed out that other NO_x species such as N_2O, N_2O_3, etc. are not detected during either adsorption of NO and NO_2 or TPD of NO and NO_2.

3.7. In situ IR characterization of NO_2 adsorbed on $BaCO_3$

In order to study the role of the $BaCO_3$ in NO decomposition, NO_x adsorbed on $BaCO_3$ experiment were performed by in situ diffuse reflectance infrared Fourier transform (DRIFT) spectroscopy. The DRIFT for $BaCO_3$ powder by introducing 2000 ppm NO and 5% O_2 in He were measured at 673 and 773 K shown in Fig. 13. Three nitrate species could be identified: bands at 1236 (w), 1507 (shoulder), 1610 (shoulder) and 1585 (s) cm^{-1} are those of a bridged nitrate [39,48]. The band at 1271 (w) cm^{-1} associated with a shoulder at 1513 cm^{-1} is a nitrate unidentate. The bands at 1550 (s), 1740 and 1765 (m) cm^{-1} can be assigned to chelating bidentate nitrate [49]. The assignment of band at 1765 (m) cm^{-1} can also correspond to free gaseous NO_2 molecular. According to the literature, the bands at 829 (w), 1054 (m) and 1480 (w) cm^{-1} are assigned to a nitrite species [44]. The formation of nitrate and nitrite species proves that NO_x (mainly NO_2 species) can be adsorbed on $BaCO_3$. Furthermore, the intensities of the bands increase when the temperature varies from 673 to 773 K, which indicate that the adsorbed capability of $BaCO_3$ is strengthened with the increase of adsorbed temperature.

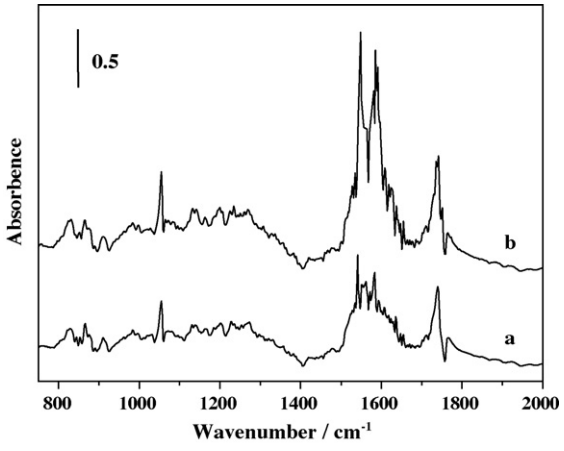

Fig. 13. DRIFT spectra on $BaCO_3$ absorbed with NO and O_2 in He (NO: 2000 ppm, O_2: 5%; (a) 673 K, (b) 773 K).

3.8. The role of $BaCO_3$

Direct decomposition of NO over perovskites-like oxides depends mainly on the number of oxygen vacancies and the redox-capability of B-site cation. Ni^{3+}–Vo–Ni^{2+} is regarded as the active sites to dissociate NO over $La_{2-x}Ba_xNiO_4$ ($x \leq 1.2$) catalysts [3,11,12,15,27]. The gaseous NO adsorbs firstly on active site like reaction (1), and dissociates into N_2 and atomic oxygen (reaction (2)). The atomic oxygen on oxygen vacancy (Ni^{3+}–O^-–Ni^{3+}) is desorbed to form O_2 ($O_{2(g)}$) with another one. Thus, the active site can be regenerated. But this process is slow and only occurs at high temperature. Iglesia et al. and Yang et al. suggested that the recycle of NO_2 (its formation and dissociation) plays an important role in the reaction over perovskite-like oxides [23,27]. The gaseous NO ($NO_{(g)}$) or adsorbed NO ($NO_{(a)}$) could react with surface oxygen to form adsorbed NO_2 ($NO_{2(a)}$) species. The desorption of $NO_{2(a)}$ species can form gaseous NO_2 ($NO_{2(g)}$). But $NO_{2(g)}$ is not detected in our experiment as shown in Fig. 12. According to the above discussion (Figs. 11–13), the basic $BaCO_3$ could adsorb intermediate NO_2 species resulting in a new catalytic way. It is suggested that the gaseous NO or adsorbed NO (Ni^{3+}–NO^-–Ni^{3+}) could react with surface oxygen (Ni^{3+}–O^-–Ni^{3+}) to form NO_2–$BaCO_3$ transition state species (nitrates or nitrites, denoted as: $(NO_2–BaCO_3)*$) resulting in regeneration of Vo (Ni^{3+}–Vo–Ni^{2+}) in the function of $BaCO_3$ described as reaction 3 and 4. In high reaction temperature, the $(NO_2–BaCO_3)*$ species is strongly unstable, and is rapidly decomposed to NO and O_2 consequently (reaction (5)). Thus, $BaCO_3$, as an assistant, takes the function of accelerating the regeneration of Vo and quickening up the run of catalytic NO decomposition recycle. It is pointed out that the number of Vo and the property of B site cation are essential factors to NO decomposition. This is maybe why $La_{0.8}Ba_{1.2}NiO_4$ performed poor activity, although there is more $BaCO_3$ phase.

The possible key reaction steps of NO decomposition in presence of $BaCO_3$ are as follows:

$$Ni^{3+}–Vo–Ni^{2+} + NO_{(g)} \rightarrow Ni^{3+}–NO^-–Ni^{3+} \quad (1)$$

$$2Ni^{3+}–NO^-–Ni^{3+} \rightarrow N_{2(g)} + 2Ni^{3+}–O^-–Ni^{3+} \quad (2)$$

$$Ni^{3+}–NO^-–Ni^{3+} + Ni^{3+}–O^-–Ni^{3+} + BaCO_3 \rightarrow 2Ni^{3+}–Vo–Ni^{2+} + (NO_2–BaCO_3)* \quad (3)$$

$$Ni^{3+}–O^-–Ni^{3+} + NO_{(g)} + BaCO_3 \rightarrow Ni^{3+}–Vo–Ni^{2+} + (NO_2–BaCO_3)* \quad (4)$$

$$(NO_2–BaCO_3)* \rightarrow BaCO_3 + NO_{(g)} + 1/2O_{2(g)} \quad (5)$$

4. Conclusion

In this study, $La_{2-x}Ba_xNiO_4$ ($x \leq 1.2$) catalysts have been prepared and characterized concerning the improvement in catalytic performance by doping Ba in direct decomposition of NO. It is found that Ba doping is highly effective for increasing NO direct decomposition activity of La_2NiO_4 catalyst. This study has revealed that $La_{1.2}Ba_{0.8}NiO_4$ shows the highest activity in direct NO decomposition even with NO of high concentration and in presence of O_2 as far as we know. It is attributed to three aspects: (1) NO adsorption test shows Ba doping results in the increasing Vo content, which increases the mobility of lattice oxygen of catalysts. These are important factors to good performance in NO decomposition; (2) with the doping of Ba, the increase in Ni^{3+} content is confirmed by the results of iodometry and H_2-TPR. Thus, the redox capability of nickel is enhanced; (3) the appearance of $BaCO_3$ phase, as NO_2 storage component, is conducive to the improvement of activity by adsorbing the intermediate NO_2 species, $BaCO_3$ plays an important role in quickening up the run of catalytic NO decomposition recycle.

Acknowledgment

This work was financially supported by the Natural Science Foundation of China and Heilongjiang Province (grant 20271019, 20676027, B200504). The authors also thank Prof. Zhen Zhao (China University of Petroleum, Beijing) for his suggestion and help with the DRIFTS analysis.

References

[1] J.W. Hightower, D.A. Van Leirsberg, in: R.L. Klimish, J.G. Larsonv (Eds.), The Catalytic Chemistry of Nitrogen Oxides, Plenum Press, New York, 1975, p. p. 63.
[2] C. Tofan, D. Klvana, J. Kirchnerova, Appl. Catal. A 223 (2002) 275.
[3] Z. Zhao, X.G. Yang, Y. Wu, Appl. Catal. B 8 (1996) 281.
[4] K.K. Hansen, E.M. Skou, H. Christensen, T. Turek, J. Catal. 199 (2001) 132.
[5] H.X. Dai, H. He, P.H. Li, L.Z. Gao, C.T. Au, Catal. Today 90 (2004) 231.
[6] R.D. Zhang, H. Alamdari, S. Kaliaguine, Appl. Catal. B 72 (2007) 331.
[7] T. Ishihara, M. Ando, K. Sada, K. Takiishi, K. Yamada, H. Nishiguchi, Y. Takita, J. Catal. 220 (2003) 104.
[8] Z.M. Liu, J.M. Hao, L.X. Fu, T.L. Zhu, Appl. Catal. B 44 (2003) 355.
[9] R.D. Zhang, A.V.H. Alamdari, S. Kaliaguine, Appl. Catal. B 64 (2006) 220.
[10] A.A. Leontiou, A.K. Ladavos, G.S. Armatas, P.N. Trikalitis, P.J. Pomonis, Appl. Catal. A. 263 (2004) 227.
[11] J.J. Zhu, Z. Zhao, D.H. Xiao, J. Li, X.F. Xie, X.G. Yang, Y. Wu, J. Mol. Catal. A 238 (2005) 35.
[12] M.A. Peña, J.L.G. Fierro, Chem. Rev. 101 (1981).
[13] H. Iwakuni, Y. Shinmyou, H. Yano, H. Matsumoto, T. Ishihara, Appl. Catal. B 74 (2007) 300.
[14] J. Liu, Z. Zhao, C.M. Xu, A.J. Duan, Appl. Catal. B 78 (2007) 61.
[15] J.J. Zhu, D.H. Xiao, J. Li, X.G. Yang, Y. Wu, J. Mol. Catal. A 234 (2005) 99.
[16] O. Kubaschewski, C.B. Alckock, P.J. Spencer, Materials Thermochemistry, 6th ed., Pergamon Press, Oxford, 1993, p. 293.
[17] Y. Teraoka, H. Fukuda, S. Kagawa, Chem. Lett. 19 (1990) 1.
[18] Y. Li, W.K. Hall, J. Catal. 129 (1991) 202.
[19] Y. Teraoka, T. Harada, S. Kagawa, J. Chem. Soc., Faraday Trans. 94 (1998) 1887.
[20] M. Iwamoto, H. Hamada, Catal. Today 10 (1991) 57.
[21] S. Xie, M.P. Rosynek, J.H. Lunsford, J. Catal. 188 (1999) 24.
[22] E. Fridell, M. Skoglundh, B. Westerberg, S. Johansson, G. Smedler, J. Catal. 183 (1999) 196.
[23] B. Moden, P.D. Costa, B. Fonfe, D.K. Lee, E. Iglesia, J. Catal. 209 (2002) 75.
[24] B.J. Adelman, G.D. Lei, W.M.H. Sachtler, Catal. Lett. 28 (1994) 119.
[25] Y. Chang, J.G. McCarty, J. Catal. 178 (1998) 408.
[26] J.A. Rodriguez, T. Jirsak, S. Sambasivan, D. Fischer, A. Maiti, J. Chem. Phys. 112 (2000) 9929.
[27] J.J. Zhu, D.H. Xiao, J. Li, X.F. Xie, X.G. Yang, Y. Wu, J. Mol. Catal. A 233 (2005) 29.
[28] M. Piacentini, M. Maciejewski, A. Baiker, Appl. Catal. B 65 (2006) 157.
[29] H. Wang, L.Y. Duan, Y.C. Xie, Chin. J. Catal. 26 (2005) 1088.
[30] F. Prinetto, G. Ghiotti, I. Nova, L. Lietti, E. Tronconi, P. Forzatti, J. Phys. Chem. B 105 (2001) 12732.
[31] J. Szanyi, J.H. Kwak, J.C. Hanson, C.M. Wang, T. Szailer, C.H.F. Peden, J. Phys. Chem. B 109 (2005) 7339.
[32] T. Szailer, J.H. Kwak, D.H. Kim, J.C. Hanson, J. Szanyi, J. Catal. 239 (2006) 51.
[33] N.W. Cant, I.O.Y. Liu, M.J. Palterson, J. Catal. 243 (2006) 309.
[34] C.M.L. Scholz, V.R. Gangwal, M.H.J.M. de Croon, J.C. Schouten, Appl. Catal. B 71 (2007) 143.
[35] G. Zhou, T. Lou, R.J. Gorte, Appl. Catal. B 64 (2006) 88.
[36] D.C. Harris, T.A. Hewton, J. Solid State Chem. 69 (1987) 182.
[37] L.K. Gushee, R. Ward, J. Am. Chem. Soc. 79 (1957) 5601.
[38] Z.L. Yu, L.Z. Gao, S.Y. Yuan, Y. Wu, J. Chem. Soc. Faraday Trans. 88 (1992) 3245.
[39] P. broqvist, H. Grönbeck, E. Fridell, J. Phys. Chem. B 108 (2004) 3523.
[40] P. broqvist, H. Grönbeck, E. Fridell, I. Panas, Catal. Today 96 (2004) 71.
[41] B.P. barbero, J.A. Gamboa, L.E. Cadús, Appl. Catal. B 65 (2006) 21.
[42] H. Lou, J. Liu, X. Liu, F. Ma, J. Chin. Rare Earth Soc. 19 (2001) 324.
[43] V.G. Milt, C.A. Querini, E.E. Miró, M.A. Ulla, J. Catal. 220 (2003) 424.
[44] K. Nakamoto, Infrared and Raman Spectra of Inorganic and Coordination Compounds, 3th ed., John Wiley & Sons press, New York, 1978.
[45] J. Rynkowski, P. Samulkiewicz, A.K. Ladavos, P.J. Pomonis, Appl. Catal. A 263 (2004) 1.
[46] R.M. García de la Cruz, H. Falcón, M.A. Peña, J.L.G. Fierro, Appl. Catal. B 33 (2001) 45.
[47] N.A. Merino, B.P. Barbero, P. Grange, L.E. Cadús, J. Catal. 231 (2005) 232.
[48] J. Szanyi, J.H. Kwak, D.H. Kim, S.D. Burton, C.H.F. Peden, J. Phys. Chem. B 109 (2005) 27.
[49] S. Hodiati, K. Vaezzadeh, C. Petit, V. Pitchon, A. Kiennemann, Catal. Today 59 (2000) 323.